HIGLY PREDICTIVE MODELLING OF ENTIRE SI SOLAR CELLS FOR INDUSTRIAL APPLICATIONS

P.P. Altermatt,[1,2] S. Steingrube,[1,2] Y. Yang,[3] C. Sprodowski,[1] T. Dezhdar,[2] S. Koc,[1]
B. Veith,[2] S. Herrman,[2] R. Bock,[2] K. Bothe,[2] J. Schmidt,[2] R. Brendel[1,2]

[1] Dep. of Solar Energy Research, Leibniz University of Hanover, Appelstr. 2, 30167 Hannover, Germany
[2] Institute for Solar Energy Research Hamelin (ISFH), Am Ohrberg 1, 31860 Emmerthal, Germany
[3] On leave from: Institute for Solar Energy Systems, Sun Yat-Sen University, 510006, Guangzhou, China

The prospective efficiency improvements due to advanced metallisation technology of industrially fabricated Czochralski (Cz) silicon solar cells are assessed by means of highly predictive numerical modelling in two- and three dimensions. The analysis shows that an improved emitter design is only possible with advanced metallisation concepts, and that about 19% efficiency can be achieved with this. Then, the fully metallised back surface field (BSF) limits cell performance. If this BSF is replaced by point contacts without substantial BSF (PERC design), the efficiency is limited to about 20% because the wafer resistivity must be 0.5 Ωcm at maximum, so Cz material has a very limited carrier lifetime due to the boron-oxygen complex. If local BSFs are formed at the rear point contacts (PERL design), higher wafer resistivities can be used, so the base operates under high-injection conditions where the boron-oxygen complex is less detrimental. However, such improvements to the rear side increase cell efficiency only substantially if the lifetime in the Cz material, in particular its interstitial oxygen density, is reduced.

1 PURPOSE

It is well known that in today's fabricated cells, improvements in the emitter increase cell efficiency the most. However, such improvements cause a higher sheet resistivity in the emitter, and to keep the resistive losses moderate, the distance between the front metal fingers needs to be made smaller. To avoid excessive shadowing, the finger width needs to be made smaller, too. Hence, substantial improvements in the emitter can only be achieved with changes to the metallisation technology (including an advanced screen-printing technology). The recent introduction of the Pluto cell to mass production is a trend-setting example [1].

Whoever accomplishes a change in metallisation can exploit benefits from a number of cell designs, not only regarding the emitter, but also the rear. This can boost cell efficiency significantly, in contrast to the gradual efficiency improvements that had been accomplished in the recent past.

When deciding for a different metallisation technology, a central question is, which cell efficiency can possibly be gained, because this limits the affordable production costs. Presently, there is a high demand for calculating prospective efficiency improvements of various cell structures. Numerical modelling is a versatile tool for this, and the purpose of this paper is to calculate the expected cell efficiency after various changes to fabrication.

2 THE NUMERICAL MODEL

The electronics industry has been applying numerical modelling successfully for decades. However, their physical models are unsuitable for Si solar cells because these models are tailored to binary-logic devices where, for example, the exact value of the minority carrier density is usually insignificant. Hence, the physical models for solar cells needed to be refined over years, involving various PV institutions. Only recently have simulations of industrial Si solar cells become highly predictive. Like in the analysis of laboratory cells, one works within the framework of the fully coupled semiconductor equations [2] in the drift-diffusion approximation, and by using Fermi-Dirac statistics [3]. Other improvements include fine-tuned models for the effective intrinsic carrier density $n_{i,eff}$ [4-6], the radiative [7] and Auger [8-11] recombination, and a mobility model that accounts for differences between majority- and minority carriers [12]. Simulation models for surface passivation [3-17] needed to be tailored to PV specific fabrication, and in some materials additional models for gettering [18,19] needed to be incorporated.

These models have recently turned out to reproduce measured I-V curves of industrially fabricated cells *without* the need to adjust input parameters. Instead, we use independently measured device properties such as dopant profiles, finger geometry, bulk lifetime, etc. and obtain satisfactory results. In addition, we are able to simulate *entire* cells, including their full metallisation geometry and their edges, by a combination of device- and circuit modelling indicated in Fig. 1. In a first step, the semiconductor device simulator simulates a minimal 2D or 3D section of the cell. This takes into account all effects in the cell's semiconductor regions, including surface recombination, contact resistance etc. The simulated I-V curve is then used as an input to the circuit

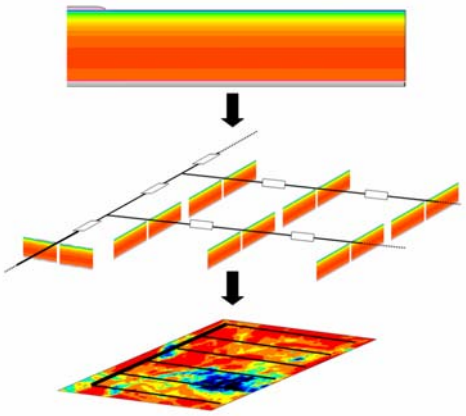

Figure 1: Flow diagram of the simulations. 2D or 3D semiconductor device simulations (top) are inserted into a circuit simulation to account for metallisation and edge effects (middle) and possibly for inhomogeneities of the cell (bottom).

simulation. The entire solar cell can be considered to consist of many of these semiconductor sections that are laid out like tiles and connected in a circuit by ohmic resistances, which represent the metallisation. If desired, semiconductor sections that are part of the bus bar, represent crystal grains with low lifetimes, or the cell's edge can be simulated and inserted in the circuit simulation at the appropriate locations. The circuit simulation requires input parameters such as metallisation geometry, finger- and busbar resistivity, etc. We use the simulator SENTAURUS [20].

3 ASSESSMENT OF LIMITING J_0 VALUES

In this Section, typical recombination losses in various device parts of present-day industrial Cz c-Si cells are assessed by means of their saturation current-density J_0. In experiment, J_0 is usually determined by means of test samples with the method of Kane and Swanson [21], e.g. by using the quasi-steady-state photo-conductance (QSSPC) method [22]. In simulations, it can either be quantified as described in Ref. [3] or by simulating a cell and integrating the recombination losses over the various device parts separately.

3.1 Emitter

Typically, emitters with a measured $J_{0,\mathrm{em}}$ values in the range of 900 – 2100 fA/cm^2 are fabricated. The emitter is contacted by screen printing and must fulfil stringent conditions, which leaves very little room for a variation of the dopant profile and accordingly for a variation of $J_{0,\mathrm{em}}$.

Our simulations reproduce the measured $J_{0,\mathrm{em}}$ well if the experimentally determined dopant profiles are used together with PV specific models for the surface recombination, as in Ref. [3]. It is imperial to use Fermi-Dirac statistics, as was justified in Ref. [3]. If Boltzmann statistics are used, e.g. with the simulator PC1D [23], the losses at the surface are usually overestimated at high N_{dop}. Our simulations reveal that the nitride layer passivates the surface so slightly that it reduces $J_{0,\mathrm{em}}$ only little. The main benefit from the nitride layer comes during firing, where hydrogen is released and passivates defects in the bulk [24].

3.2 BSF

The Al-alloyed BSF has typically measured $J_{0,\mathrm{BSF}}$ values that are between 600 fA/cm^2 and 900 fA/cm^2. Reports of lower values are sometimes questionable, for two main reasons: (i) the method of Kane and Swanson ideally requires symmetric samples but the QSSPC set-up needs one side of the samples unmetallised, so the Al is either etched off or $J_{0,\mathrm{BSF}}$ is inferred from asymmetrical samples without in-depth analysis; (ii) $J_{0,\mathrm{BSF}}$ is deduced from the rear surface recombination velocity, S_{rear}, inferred from quantum efficiency measurements and hence is sensitive to the assumed light-trapping calculations.

The simulation of the Al-BSF has been a challenge: using the experimentally determined Al profile, far too low $J_{0,\mathrm{BSF}}$ values are obtained. For example, the typical, 10 µm deep Al profile shown in Fig. 2 yields $J_{0,\mathrm{BSF}}$ = 290 fA/cm^2 instead of the measured 650 fA/cm^2. Recent investigations [25] revealed that an upper limit of the average lifetime within the Al-BSF is about 130 ns, well below its Auger limit. This indicates that defects are introduced during alloying which limit the SRH recombination in the bulk. Trial-experiments with Al-doped Cz material show a lifetime according to

$$1/\tau_{\mathrm{SRH}}\,[\mu\mathrm{s}] = 2.8339\times10^{-24} N_{\mathrm{acc}}{}^{1.5048}\, f, \qquad (1)$$

with f = 1, probably caused by the formation of aluminium-oxygen (Al-O) defect complexes. N_{acc} denotes the acceptor density. Applying Eq. (1) to simulations of the Al-BSF often results in far too high $J_{0,\mathrm{BSF}}$ values. This is not surprising because, during the fabrication of the Al-BSF, the temperature is usually kept below 900°C and peaks only for a few seconds. If we use $f = 2\times10^{-6}$ in Eq. (1) we reproduce the measured $J_{0,\mathrm{BSF}}$ of both, the original and the etched-back profiles shown in Fig. 2. Note that this SRH lifetime (indicated by the line in Fig. 2) is consistent with the above-mentioned upper limit of 130 ns. Despite of this consistency between the model and $J_{0,\mathrm{BSF}}$ measurements, Eq. (1) together with f is not necessarily the τ_{SRH} limit in fabricated Al-BSFs: other types of defects may dominate the SRH recombination, for example crystal defects incorporated during re-crystallisation, whose density may be independent of the Al density. We use Equ. (1) and f as a sophisticated guess on the ground that (i) a certain number of Al-O defects are generated also at lower temperatures than 900°C, because they are thermally activated; and (ii) the lifetime is rather constant over most of the Al-BSF volume, so the exact cause for it has only minor consequences for $J_{0,\mathrm{BSF}}$.

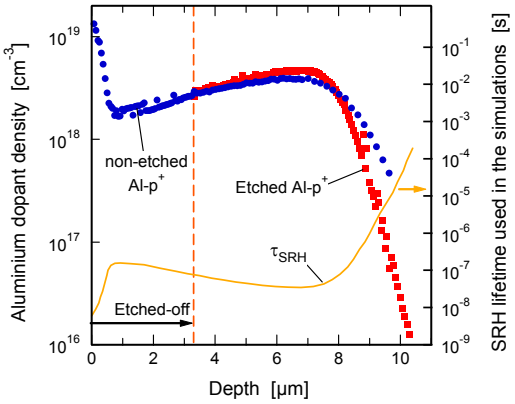

Figure 2: Typical Al profile of a back surface field (BSF), measured by the ECV technique [26] (blue, round symbols), and after etching off 3.3 µm by KOH (red square symbols). The $J_{0,\mathrm{BSF}}$ values are reproduced by the numerical simulations using the SRH lifetime of Eq. (1) and a factor $f = 2\times10^{-6}$ (line).

3.3 Base

In experiment, the recombination losses in the base are not quantified by means of $J_{0,\mathrm{base}}$ but by means of the bulk lifetime τ_{bulk}. To compare the losses of all device parts, we express $J_{0,\mathrm{base}}$ analytically in relation to τ_{bulk} using

$$J_{0,base} = \frac{q n_{i,eff}^2 W}{N_{acc}\tau_{bulk}}, \qquad (2)$$

which is valid as long as the diffusion length is larger than the cell's thickness W. τ_{bulk} is approximately τ_{SRH} within the N_{acc} range considered here. If the cells are fabricated on Cz material, τ_{SRH} is limited by the boron-

oxygen (B-O) complex described by the SRH parameters [27-29]

$$\tau_{n0}\,[\mathrm{s}] = 4.02024\times10^{45}\,[\mathrm{B_s}]^{-0.824}\,[\mathrm{O_i}]^{-1.748}\,m \quad (3a)$$
$$\tau_{p0}\,[\mathrm{s}] = 10\,\tau_{n0} \quad (3b)$$
$$E_d\,[\mathrm{eV}] = E_c - 0.41\,, \quad (3c)$$

where $[\mathrm{B_s}] = N_{\mathrm{acc}}$ is the substitutional boron density, $[\mathrm{O_i}]$ is the interstitial (not precipitated) oxygen density in cm^{-3}, m is an improvement factor, which depends on the fabrication conditions and is usually near 2, and E_d is the defect's energy level in respect to the conduction band edge E_c. At low injection conditions, τ_{SRH} is limited by τ_{n0}, at high-injection levels by $\tau_{n0} + \tau_{p0}$, so τ_{SRH} increases tenfold going from low- to high-injection conditions. This can be expressed by the SRH formula and the appropriate approximations for n_1 and p_1:

$$\tau_{SRH} = \tau_{p0}\left(\frac{1}{N_{acc}/\Delta n + 1} + \frac{1}{10}\right). \quad (4)$$

Because the injection conditions in the base depend on the external bias V, an assessment of J_0 in the base is rather intricate. In Fig. 3, $J_{0,\mathrm{base}}$ is computed with $W = 180$ µm and at the external biases $V_{mpp} = 500$mV and 600 mV, using

$$pn = n_{i,eff}^2 e^{V/V_{th}} \rightarrow$$
$$\Delta n \approx n = \frac{-N_{acc} + \sqrt{N_A^2 - 4n_{i,eff}^2 e^{V/V_{th}}}}{2} + n_{sc} \quad (5)$$

in low injection. V_{th} is the thermal voltage, and the electron density at short-circuit condition n_{sc} is chosen as 9×10^{12} cm^{-3}, which is a typical value. At high-injection, simulated values are used.

A view features can be seen in Fig. 3.

- $J_{0,\mathrm{base}}$ depends only weakly on N_{acc} at low-injection conditions, because N_{acc} is partly cancelled out in combining Eqs. (2) and (3a). However,
- $J_{0,\mathrm{base}}$ decreases strongly when going towards high-injection conditions, i.e. with increasing V or decreasing N_{acc}. The voltage-dependence implies that $J_{0,\mathrm{base}}$ is higher at MPP than at open-circuit conditions, which may lower the fill factor FF.
- $J_{0,\mathrm{base}}$ depends strongly on $[\mathrm{O_i}]$. Usually, Cz materials with $[\mathrm{O_i}]$ in the range of $(7 - 8)\times10^{17}$ cm^{-3} are fabricated. The action of oxygen on τ_{SRH} via the improvement factor m can be weakened for example by fast cooling conditions after the phosphorus diffusion. Curing [30,31] may be an other alternative to reduce $J_{0,\mathrm{base}}$.

Fig. 3 indicates that $J_{0,\mathrm{base}}$ is lower than $J_{0,\mathrm{BSF}}$ in most of today's industrially fabricated cells on 5 Ωcm material. However, it is quite close to $J_{0,\mathrm{BSF}}$ and therefore needs to be considered when deciding on new cell designs.

To sum up the assessment of typical industrial cells, Fig. 4 shows results of numerical simulations done with the BSF shown in Fig. 2 (non-etched), and a heavy (moderate) emitter dopant profile, resulting in $J_{0,\mathrm{em}}$ = 1800 fA/cm² (1100 fA/cm²). Note that the efficiency gain from a 1 Ωcm to a 10 Ωcm base is rather small because V_{mpp} is rather low (near 500 mV) so the benefits from high-injection in the base cannot be exploited. This example shows that specific changes in material or cell design need to be considered in context of the *entire* cell, not only of the part that is changed, as will be discussed in more detail in the following Section.

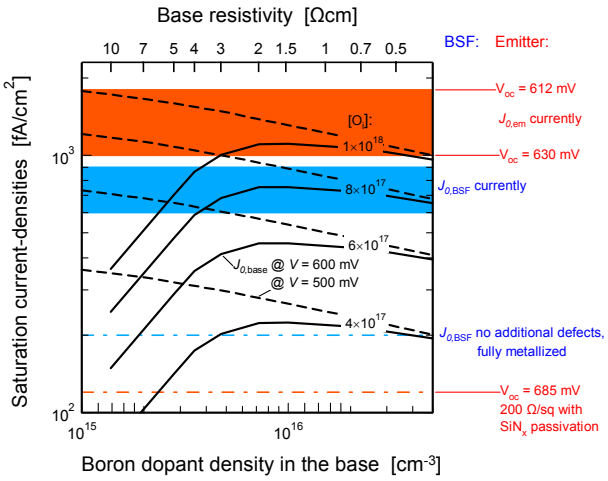

Figure 3: $J_{0,\mathrm{base}}$ values for various oxygen densities, calculated at a bias of 500 mV (dashed) or 600 mV (solid lines) by means of Eqs. (2) – (5) and numerical simulations. The horizontal lines and solid areas indicate J_0 values of the emitter and the BSF, respectively (the weak injection-dependence of $J_{0,\mathrm{BSF}}$ is ignored). The V_{oc} capabilities of the emitter are calculated with the Shockley equation using ideality factor 1.

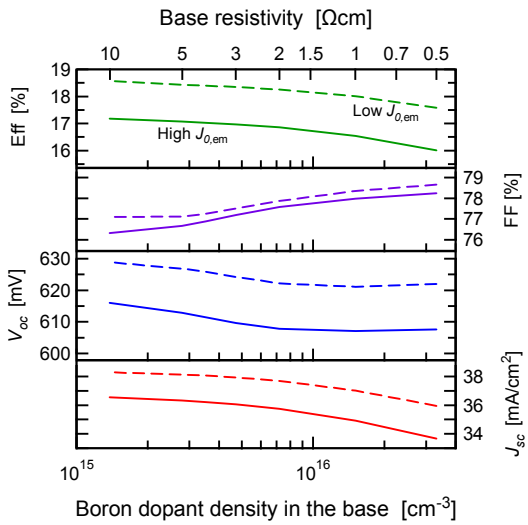

Figure 4: Simulated I-V parameters of a typical industrial cell with a heavily diffused emitter (solid lines) and an uncommonly moderately doped emitter (dashed lines). Their $J_{0,\mathrm{em}}$ values are at the higher or lower present limits, indicated by the red area in Fig. 3. The Cz wafer is 180 µm thick and has an oxygen density of 7×10^{17} cm^{-3} (solid lines) or 6×10^{17} cm^{-3} (dashed lines). The front fingers are 2.5 mm apart, and the total shading is 6%. These parameters vary among different cell manufactures; some may have a relatively high V_{oc} but a lower FF, others may have higher J_{sc} values e.g. due to thicker wafers, etc.

4 SELECTIVE EMITTERS

In order to optimise cells, it is beneficial to reflect on the following two questions: what are the main mechanisms that determine the J_0 values of various device parts? And how can they be exploited to arrive at optimised cell designs?

In dopant-diffused regions, where low-injection conditions prevail at all V, the SRH recombination rate is limited by the minority carrier density c_{min}. A higher doping reduces c_{min} and, in turn, the SRH losses, as for example at the metal contact. However, if this were the only main mechanism that determines J_0, the depth of the BSF would not influence $J_{0,BSF}$ while, in reality, a deeper BSF is substantially better. The second mechanism that comes into play is the transport properties: for SRH recombination to occur there needs to be a steady *supply* of minority carriers. A deeper BSF has inferior transport properties than a shallow one, so the minority carriers have difficulties reaching the metal contact to recombine. Simulations with the model of Section 2 show that an ideal, 12 µm deep, fully metallised Al-BSF without additional defects (f = 0 in Eq. 1) may reach a $J_{0,BSF}$ value down to about 200 fA/cm^2 (see Fig. 3). Boron-doped BSFs, which are known for their Gaussian dopant profiles and very low defect densities, may reach similarly low values (100 fA/cm^2) if fully metallised [32].

In contrast to the BSF, the emitter at the front surface requires good transport properties to collect the carriers that are photo-generated near the surface. This is the main reason why $J_{0,em}$ cannot be minimized and why cell design is not trivial. Because transport and recombination are strongly coupled in the semiconductor equations, the emitter is an intricate trade-off between these two phenomena. And it is also the reason why, in present industrial cell design, $J_{0,em}$ is usually larger than $J_{0,BSF}$.

One way to improve the emitter is to make it selective, i.e. that it is heavily diffused only under the metal fingers. Many ways have been investigated to achieve this. As long as the heavy local diffusions under the finger do not dominate $J_{0,em}$, the same cell efficiency can be achieved regardless in which way selectivity is achieved. We demonstrate how improvements of the emitter affect the cell's performance by gradually etching the surface of the emitter [33] used in Fig. 4 (having $J_{0,em}$ = 1800 fA/cm^2) or of a deeper emitter diffusion (having $J_{0,em}$ = 1300 fA/cm^2). The I-V parameters are monitored in Fig. 5. The remaining simulation parameters are the same as in Fig. 4, e.g. the emitter is passivated with SiN_x with n = 2.05 [3]. However, the metal fingers are kept 1 mm apart, are 48 µm wide, and their aspect ratios are sufficiently high as to maintain the usual resistance.

It can be observed in Fig. 5 that etching off the most heavily part of the diffusion within the first 80 nm (40 nm in case of the deeper diffusion) leads to a lower V_{oc}, because the transport properties from the surface to the junction improve (leading to some improvement of J_{sc}) while N_{peak} and hence S_{p0} stay rather constant, so more carriers recombine. This may have been the reason why no improvement was observed in early experiments [34]. Etching the emitter deeper causes N_{peak} to lower substantially; the SiN_x passivation becomes effective and both V_{oc} and J_{sc} improve [35]. Etching further improves cell efficiency only until $J_{0,em}$ has become considerably smaller than $J_{0,BSF}$ + $J_{0,base}$, because cell efficiency depends on the sum $J_{0,em}$ + $J_{0,BSF}$ + $J_{0,base}$. In the case of this cell example, a maximal efficiency to about 19 % is expected by improvements of the emitter and the front metallisation. Then, $J_{0,em}$ = 120 fA/cm^2 with a SiN_x passivation, see Fig. 3.

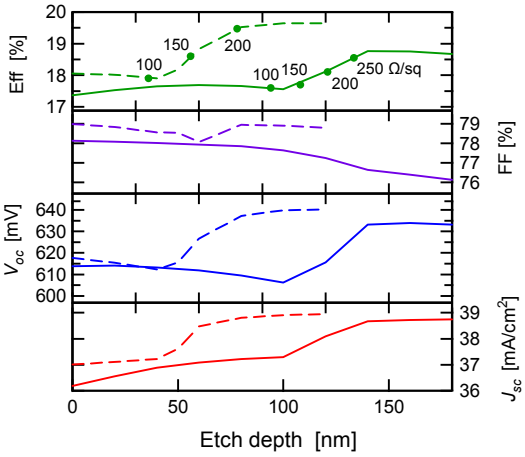

Fig. 5: Performance of cell made with the heavily diffused emitter of Fig. 4 (solid line), and a lighter but more deeply diffused emitter (dashed line), as gradually etched at its surface. The numbers at the efficiency curves indicate the emitter's sheet resistivity. The finger distance is 1mm, and the total shading is 6%.

From Figs. 3 and 5 it is obvious that a cell with an improved emitter is soon limited in its performance by the BSF. Hence, the next Section deals with improvements to the rear.

5 PASSIVATED REAR

For a selective emitter to be beneficial, the metallisation technology has to be changed as outlined in the Introduction and the proceeding Section. Once a new metallisation technology is introduced to production, one is able to improve the rear in a similar manner as the emitter, leading to a further efficiency boost. In order to evaluate such an improvement, we now discuss numerical, three-dimensional simulations of a PERC structure [36], i.e. the cell's undiffused rear surface is passivated and locally contacted by point metal contacts without significant BSF.It is well known that the performance of PERC and similar cell structures reacts sensitively to the effective recombination velocity S_{eff} at the rear surface [37]. To look at prospects of an industrial environment, we derived simulation parameters for a fired Al_2O_3/SiN_x double layer from test samples [38]. The Al_2O_3 layer was deposited on both sides of a 1.5 Ωcm p-type float-zone (FZ) Si wafer by the atomic layer deposition (ALD) technique. As the deposition rate of ALD is very low, the thickness of the Al_2O_3 layer is set at 3.6 nm. To improve the firing stability of this ultra-thin Al_2O_3 film, a 75 nm thick SiN_x layer is deposited on top of the Al_2O_3 by plasma-enhanced chemical vapour deposition [38]. The measured S_{eff} is near 15 cm/s before firing and near 50 cm/s after firing at 830ºC in a standard conveyor-belt furnace [38]. In comparison, unfired SiN_x has a S_{eff} value that is typically near 100 – 200 cm/s [39] in the relevant injection conditions.

These parameters are inserted in a three-dimensional, numerical simulation of a PERC cell. Its front emitter of Section 4 is etched to 200 Ω/sq and passivated by SiN_x. At the rear, the metal contacts have a diameter of 85 µm,

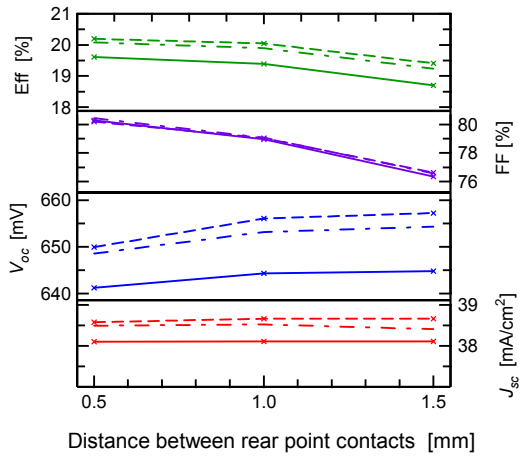

Fig. 6: Simulation results of a PERC cell made of 0.5 Ωcm Cz material. At the rear, the cell has point contacts with a diameter of 85 µm and is passivated by an Al_2O_3/SiN_x stack. Solid line: Cz material with an oxygen density $[O_i] = 6\times10^{17}$ cm^{-3}; dashed line: $[O_i] = 4\times10^{17}$ cm^{-3}; dashed-dotted line: $[O_i] = 4\times10^{17}$ cm^{-3} but passivated solely by SiN_x.

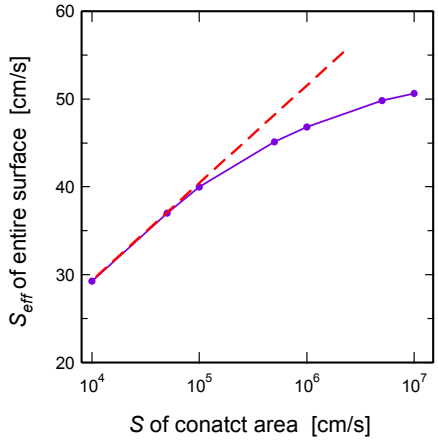

Fig. 7: The effective surface recombination velocity, $\langle S_{eff}\rangle$, averaged over the rear surface, as a function of S_{eff} of the contact area, simulated numerically in three dimensions with a distance between the circular contacts of 1 mm. To show the effect, S_{eff} of the passivated part of the surface is chosen as 10 cm/s.

while the rest of the surface is passivated by the fired Al_2O_3/SiN_x passivation layer. Figure 6 shows the simulation results in dependence of the distance between the rear contacts, and assuming a contact resistivity of 5 mΩcm^2. It is apparent that the cell has a rather modest performance compared to its sophisticated fabrication. In the PERC design, a maximal wafer resistivity of 0.5 Ωcm must be used, and it follows from Fig. 3 that the efficiency is limited by $[O_i]$ in the Cz material. Therefore, the benefits of the Al_2O_3/SiN_x stack are modest compared to a standard SiN_x passivation (dash-dotted line compared to dashed line), although Cz material with a very low $[O_i] = 4\times10^{17}$ cm^{-3} is assumed in Fig. 6. It is obvious that a PERC design on Cz material has limited capabilities.

For further efficiency improvements, the rear contacts must be made with a BSF, resulting in a PERL design [40]. In this way, wafer material with a higher resistivity than 0.5 Ωcm can be used. Laser fired contacts are one possibility. However, laser doping often creates rudimentary BSFs, and the question arises how the effective recombination velocity $\langle S_{eff}\rangle$, averaged over the entire rear surface, depends on the local BSFs. Fig. 7 gives an idea. A contact without BSF (PERC design) has an effective surface recombination velocity S_{eff} of 10^7 cm/s (thermal velocity). If a BSF is formed, S_{eff} of the contact area lowers gradually with a larger depth of the BSF. However, $\langle S_{eff}\rangle$ does not lower as much as is the case at low S_{eff} (where $\langle S_{eff}\rangle$ lowers as indicated by the red dashed line). The reason for this is that the recombination at high S_{eff} values is limited by the supply of carriers required for recombination (second mechanism discusses in Section 4) and not by the minority carrier density near the contact. In terms of the recombination mechanisms outlined in Section 4, the contacts of the PERC cell are already protected by a "virtual BSF", not made of a dopant profile, but by diffusion-limitation in the base.

The optimum PERL design depends on the passivation quality of the surface, the formation of the local BSF, the contact resistivity and on the transport properties in the base. An optimised PERL cell is able to have an V_{mpp} towards 600 mV on Fig. 3 and hence to exploit the benefits of the injection-dependent lifetime of the B-O complex in Cz material. However despite the optimisation efforts, its efficiency stays limited by the Cz material, which possibly means by a long-term contract with the Cz wafer supplier, as is apparent in Fig. 3.

Due to the limitations of the CZ base material, it may be sufficient to choose a full-area BSF without additional defects, contact it by metal fingers and passivate its surface by SiN_x.

8 KEY POINTS

- The emitter limits cell performance in most Si cells fabricated industrially on Cz material. Substantial improvements of the emitter can only be achieved with changes to the metallisation technology (including an advanced screen-printing technology). Typical cells may be improved by a better emitter design to about 19% efficiency at maximum.
- This is so because the BSF then limits cell performance. However, the same advanced metallisation technology enables manufacturers to improve the design of the rear as well. PERC designs are limited to about 20% efficiency on usual Cz material. To improve cell efficiency beyond 20%, local BSFs must be formed underneath the metal contacts so Cz materials with higher resistivity can be used.
- However, such improvements to the rear side only lead to substantial efficiency improvement if the lifetime in the Cz material, in particular its interstitial oxygen density, is reduced. See Figure 3 for an overview.

REFERENCES

[1] Z. Shi et al, 34th IEEE PVSC (2009), in print.
[2] W. van Roosbroeck, Bell Sys. Tech. J. 29 (1950) 560.
[3] P P. Altermatt et al., J. Appl. Phys. 92 (2002) 3187.
[4] P. P. Altermatt et al, J. Appl. Phys. 93 (2003) 1598.

[5] A. Schenk, J. Appl. Phys. 84 (1998) 3684.
[6] S. W. Glunz et al, Proc. 17th EU PV Conf. (2001) 1391.
[7] T. Trupke et. al., J. Appl. Phys. 94 (2003) 4930.
[8] P.P. Altermatt et al, J. Appl. Phys. 82 (1997) 4938.
[9] S. W. Glunz, et al, J. Appl. Phys. 86 (1999) 683.
[10] J. Schmidt et al, J. Appl. Phys. 88 (2000) 1494.
[11] M.J. Kerr, A. Cuevas J. Appl. Phys. 91 (2002) 2473.
[12] D. B. M. Klaassen, Solid-State Electron. 35 (1992) 953 and 961.
[13] A.G. Aberle et al, J. Appl. Phys. 71 (1992) 4422.
[14] S.J. Robinson et al., J. Appl. Phys. 78 (1995) 4740.
[15] P.P. Altermatt et al, 21st EU PV Conf. (2006) 647.
[16] J. Schmidt et al, Appl. Phys. Lett. 71 (1997) 252.
[17] A.G. Aberle, Prog. PV 8 (2000) 473.
[18] T. Weber et al, Proc. 21st EU PV Conf. (2006) 1486.
[19] M. Blazek et al, Proc. 23rd EU PV Conf. (2008) 1637.
[20] Sentaurus, Manual Version 2008.09, Synopsys Inc., Mountain View, CA, 2008.
[21] D.E. Kane and R.M. Swanson, Proc. 18th IEEE PVSC (1985) 578.
[22] R.A. Sinton, A. Cuevas, Appl. Phys. Lett. 69 (1996) 2510.
[23] PC1D version 5.9, D.A. Clugston, P.A. Basore, Proc. 26th IEEE PVSC (1997) 207. http://sourceforge.net/projects/pc1d/
[24] M. Bähr et al, Proc. 19th EU PV Conf. (2004) 955.
[25] J. Schmidt et al, 34th IEEE PVSC (2009), in print.
[26] R. Bock et al, 23rd EU PV Conf. (2008) 1510.
[27] K. Bothe at el, Prog. PV 13 (2005) 287.
[28] J. Schmidt, A. Cuevas, J. Appl. Phys. 86 (1999) 3175.
[29] S. Rein, S.W. Glunz, Appl. Phys. Lett. 82 (2003) 1054.
[30] A. Herguth et al, Prog. PV 16 (2008) 135.
[31] B. Lim et al, Phys. Stat. Sol. (RRL) 2 (2008) 93.
[32] N.-P. Harder et al, 19th EU PV conf. (2004) 828.
[33] A. Bentzen at al, Prog. PV 15 (2007) 281.
[34] Mardesich, 15th IEEE PVSC (1981) 446.
[35] S.R. Wenham et al, 18th IEEE PVSC (1985) 1008.
[36] A.W. Blakers et al, Appl. Phys. Lett. 55 (1989) 1363.
[37] A.G. Aberle, R. Hezel, Prog. PV 5 (1997) 29.
[38] J. Schmidt et al, Phys. Stat. Sol. (RRL) 3 (2009) 287.
[39] M.J. Kerr, A. Cuevas, Sem. Sc. Tech. 17 (2002) 166.
[40] A. Wang et al, J. Appl. Phys. 57 (1990) 602.